In: Plasmons: Theory and Applications
Editor: Kristina N. Helsey
ISBN: 978-1-61761-306-7

Chapter 9

PLASMONIC PHENOMENA IN NANOARRAYS OF METALLIC PARTICLES

Victor Coello[1], Rodolfo Cortes[1], Paulina Segovia[2], Cesar Garcia[2] and Nora Elizondo[2]

[1]Centro de Investigación Científica y Educación Superior de Ensenada (U. Monterrey). Km 9.5 Carretera Nueva al Aeropuerto. PIIT. C.P 66629. Apodaca NL. México

[2]Doctorado en Ingenieria Fisica Industrial. FCFM UANL. Ciudad Universitaria, Pedro de Alba S/N. San Nicolas de los Garza NL. Mexico

Current experimental and theoretical investigations of plasmonic phenomena are indented to be the basis for miniaturization of photonics circuits with length scales much smaller than currently achievable, inter-chip and intra-chip applications in computer systems, and bio/sensor-systems. In this chapter experiments and numerical developments conducted to the understanding of this area are outlined. We focus our attention in the interaction of Surface Plasmon Polaritons (SPP) with arrays of nano-particles. Numerical simulations and experimental results of different SPP elastic (in-plane) scattering orders, and the operation of simple plasmonic devices are presented. Furthermore, non-linear microscopy, with a tightly focused laser beam scanning over a sample surface with different densities of nano-particles is presented. Finally, a scanning near-field microwave microscope is presented as an alternative technique that is reliable enough to be used as a check of potential plasmonic components that are based on nano-particle arrays. In general, the stability with respect to geometrical parameters and dispersion were the main features investigated in all the presented plasmonic phenomena.

1. INTRODUCTION

Current progress in optics of surface plasmon polaritons (SPPs) [1] offers new and broad ranges of scientific and technological perspectives. For instance, SPP are applied to efficiently channel light using scatterers in subwavelength structures [2]. This could lead, in

principle, to a novel generation of nano-optics circuits. This atractive idea is based on the similitude between SPPs and waves propagating in planar waveguides since both are two dimensional waves propagating in the surface. However, one has to born in mind that this similitude stops here. SPP field have its maximum intensity at the surface plane, in contrast with the (two dimensional) guided waves in integrated optics. Moreover, it is easier to scatter SPP out of the plane than along to it. Actually, as a SPP field is strongly confined in the direction perpendicular to the surface, a direct observation of SPP localization is only possible by means of scanning near-field optical microscopy (SNOM) techniques [3]. Near-field optical microscopy of SPPs has corroborated the existence of both weak and strong SPP localization [4]. However a local control (at a desirable surface place) of such SPP optical enhancement started to take form only with the birth of the two-dimensional optics of SPPs [5]. The so called Plasmonics has as a purpose the manipulation and controlling of SPP beams along the surface plane by using artificially created nano-components. In particular, metallic nanoparticle arrays played an important role for the development of novel plasmonic structures [5]. Artificially fabricated SPP nano-optical structures such as nano-bumps acting as a nanolens (focusing the SPP field) have been investigated for different films and wavelengths [5]. In general, working in optics in the nano-scale regime is not trivial. Structures smaller than the wavelength, may not lead to the expected results and the investigations revealed several features such as wavelength dispersion and stability (with respect to geometric parameters) of the nano-components that still have to be elucidated. The studies are well complemented by using numerical simulations. For example, an scalar multiple-scattering approach was used for simulations of SPP optical nano-components [6] and photonic band gap structures formed by sets of individual scatterers [7]. Later, the approach has been extended into a vector dipolar multiple-scattering theory [8] and used to calculate SPP scattering produced by band-gap structures and for modelling the operation of a SPP interferometer formed by equivalent scatterers lined up and equally spaced [9]. Another interesting approach, for the sub-wavelength studies, is the use of the microwave radiation. The first proposal for a scanning near field microwave microscope (SNMM) came from Ash and Nichols in 1972 [10]. Since then, the technique has demonstrated its potential in areas such as magneto-resistivity characterization, superconductivity, and dielectric constant of individual samples [11,12]. Recently, it was proposed a simple SNMM designed to adopt dissimilar illumination operations modes and with capabilities for studies of potential two-dimensional optical devices [13]. In this work, we present an overview of some of the problems, developments and current progress related with our research in the surface polariton nano-optics. We begin with an introduction to SPPs in section 2. Experimental results on SPP localization exhibited in a metallic surfaces covered with nano-particles will be presented in section 3. Direct evidence of strong and spatially localized SH enhancement in random metal nanostructures is presented in section 4. Section 5 describes a multiple scattering model that was used for simulation of SPP elastic scattering. In section 6, the above mentioned model was extended into a vectorial dipolar model. Thus, the operation of a plasmonic line mirror formed by equivalent nano-particles lined up and equally spaced was analyzed. The effects of SPPs in artificially nanostructured surfaces will be discussed in section 7. A near-field microwave technique used as an experimental approach for checking potential two-dimensional nano-SPP components will be analysed in section 8. Finally, in section 8, the conclusions are outlined.

2. SURFACE PLASMON POLARITONS

SPPs are oscillations of surface electron charge density that can exist at a metal/dielectric interface (Figure 1). Associated with them, there exists an electromagnetic field that propagates along the interface exhibiting exponential decays perpendicular to it. Therefore, SPPs show a high sensitivity to surface properties such as roughness and surface adsorbates [14]. As it is characteristic for evanescent fields [15], for the SPP to exist, the wavenumber associated with it must be larger (in absolute value) than the light wavenumber in the neighbour media. Surface polaritons obey Maxwell's equations and they do represent (quasi) two-dimensional waves. The electromagnetic derivation of the SPP modes results in the fact, that such modes are possible only for *p*-polarization of light (TM-waves), since *s*-polarized waves (TE) do not satisfy the boundary conditions. Due to their electromagnetic nature, it is not difficult to infer that SPPs can diffract, reflect, and interfere. Those properties are clearly exhibited in the course of SPP scattering. Scattering of SPPs is usually caused by randomly placed surface imperfections (as even the most carefully prepared surfaces are not completely flat). Hereafter, we should distinguish between two kinds of SPP scattering: *inelastic and elastic SPP scattering*. For *inelastic scattering*, we will consider, propagating field components scattered away from the surface decreasing the total energy stored in SPPs. *Elastic scattering* occurs when SPPs are scattered by surface imperfections *along the surface plane*, i.e. into other SPPs preserving the total SPP energy. Concerning the mechanisms for SPP excitation, two techniques have been extensively developed: excitation by means of light, and excitation by means of electrons. SPP excitation by electrons is beyond the scope of this work (an overview can be found in Ref. 14). Otto and Kretschmann configurations[1] are the mechanism most widely used for SPP excitation by light. They include a dielectric-metal-air system, in which a light beam is impinging on the metallic surface under an angle larger than the *critical angle*. The excitation occurs at the interface between air and metal, and is recognized as a minimum in the angular dependence of the reflected beam power. An angular spectra analysis of SPP excitation allows one to deduce the SPPs characteristics, whose knowledge is indispensable for any kind of SPPs studies. However, those configurations have some drawbacks such as the separation of the source and plasmonic devices on different chips, and the large size of the prism couplers that make them not suitable for photonic integrated circuits. An alternative is the use of a normal incident light to excite the SPPs through a ridge [16] or subwavelength-hole arrays [17,18] located at the top of an air/metal interface. Such SPP launching mechanisms have been used for quantitative experimental analysis of a SPP interferometer [16], nano-parabolic chains [19], and testing of refractive plasmonic structures [20].

2.1. Surface Polaritons Properties

In order to show the SPP characteristics, first let us consider the interface between two semi-infinite media as air-metal. The SPP electric field existing in such a system (Figure 1) can be represented as:

$$E(x,y) = E_0 e^{i\beta\cdot\hat{x}} \cdot e^{-\gamma\cdot\hat{z}}, \tag{1}$$

which is an electromagnetic mode propagating in the *x*-direction along the surface and with an exponential decay perpendicular (*z*-direction) to it (Figure 1).

The SPP wave vector, β, and the air decay constant, γ, are derived through the use of Maxwell`s equations and the boundary conditions, yielding the expressions:

$$\beta = \frac{2\pi}{\lambda_0}\sqrt{\frac{\varepsilon_m}{1+\varepsilon_m}}\,,\quad \gamma = \sqrt{\beta^2 - k_0^2}\,, \tag{2}$$

being λ_0 the incident wavelength, ε_m the dielectric constant of metal, and k_0 the incident wave number. The SPPs modes have an exponential decay into each of the media, being then the SPP decay constant, γ_m , in the metallic medium given by:

$$\gamma_m = -\sqrt{\beta^2 - \varepsilon_m k_0^2}\,. \tag{3}$$

Other important SPP characteristics are, in turn, the *SPP wavelength*,

$$\Lambda_{SPP} = \frac{2\pi}{\beta}\,, \tag{4}$$

the *propagation length* i.e.: the length at which the intensity decreases to 1/*e* (along the surface),

$$L_{SPP} = \frac{1}{2\beta_{im}}\,, \tag{5}$$

with β_{im} being the imaginary part of β, and *the penetration depth* i.e.: the length (perpendicular to the surface) at which the field amplitude decrease to 1/*e*. It is given by:

$$d_1 = \frac{1}{\gamma}\ \text{(air)},\qquad d_2 = \frac{1}{\gamma_m}\ \text{(metal)}. \tag{6}$$

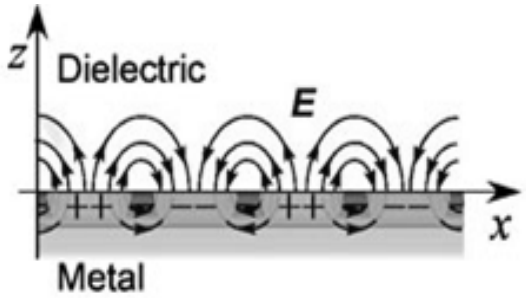

Figure 1. Schematic representation of a SPP-field (*E*) that exists at a metal/dielectric interface (*XZ* plane)

3. SPP LOCALIZATION

SPP localization is difficult to achieve since even for rough films it is not an automatically obtained effect [4,14]. It is quite difficult to find media in which one can get short mean free paths. One cannot make the volume fraction of scatterers larger and larger, since this leads not only to elastic but also to inelastic SPP scattering which may result that the optical signal will be dominated by propagating components. Apparently, to optimize the amount of scattering, it is necessary a large volume of scatterers whose sizes should approximately correspond to the SPP wavelength, λ_{SPP}. Scatterers smaller (in size) than λ_{SPP} are necessary for the near-field interactions responsible of the SPP confinement whereas those bigger than λ_{SPP} would result in strong multiple scattering indispensable for the SPP localization to occur. Then, in order to observe strong localization, ideally one would like to have a medium which scatters light very strongly and preferably with negligible absorption. Under similar sample conditions like the ones just above described (Figure 2a), direct observation of SPP localization, in the form of bright round spots, was obtained (Figure 2b). The metallic films were fabricated by means of thermal evaporation technique. The rough gold films were evaporated on the base of a glass prism which had previously been covered with a sublayer of colloidal gold particles (diameter ~ 40 nm) dried up in atmosphere. Therefore, the introduced surface roughness was randomly distributed along the sample surface. SPPs were resonantly excited by means of the Kretschmann configuration. The position of such spots resulted to be angle dependent and not correlated to surface topography. The size of the bright spots was estimated at ~300-400 nm (Figure 3). The observations were directly recorded by use of scanning near-field optical microscopy (SNOM) [3] and related to the phenomenon of strong SPP localization [4,14]. The images exhibited an enhancement ratio up to 5 times the background signal (Figure 3).

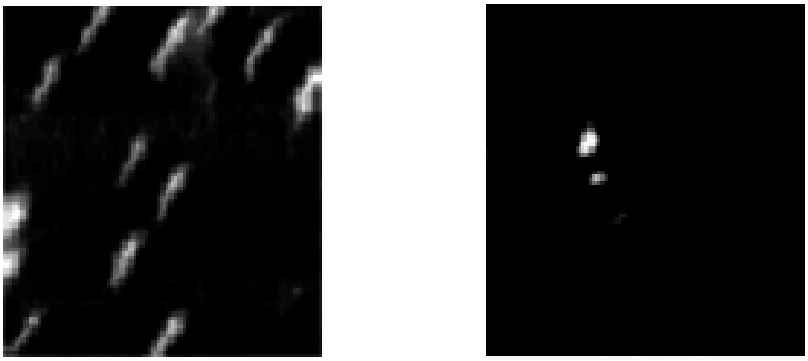

(a) (b)

Figure 2. Gray-scale topographical (a) and near-field optical (b) images of 4.5×3.6 μm^2 obtained with the gold film with nano-particles randomly distributed. The maximum height surface roughness in the topographical image is ~ 42 nm. Contrast of the optical images is ~ 98%

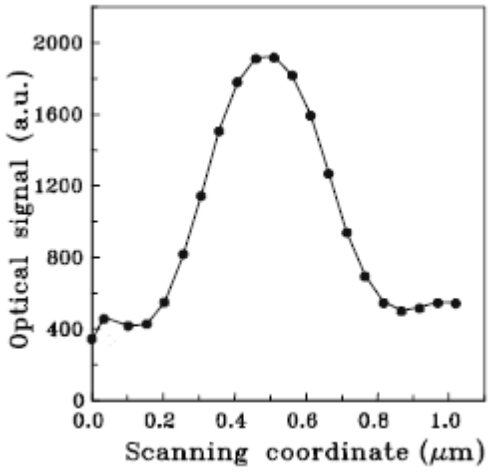

Figure 3. Horizontal cross section of the near-field optical image of the bigger bright spot shown in Figure 4 (b)

4. SECOND-HARMONIC FAR-FIELD MICROSCOPY OF LOCALIZED SPPS

Novel optical phenomena arising from the propagation of SPPs at a weakly-corrugated metal surface originated original contributions in the area of SPP-enhancement of second harmonic diffraction [21,22]. The experimental setup (Figure 4) used, for this kind of experiments, was a so called second-harmonic scanning optical microscope (SHSOM).

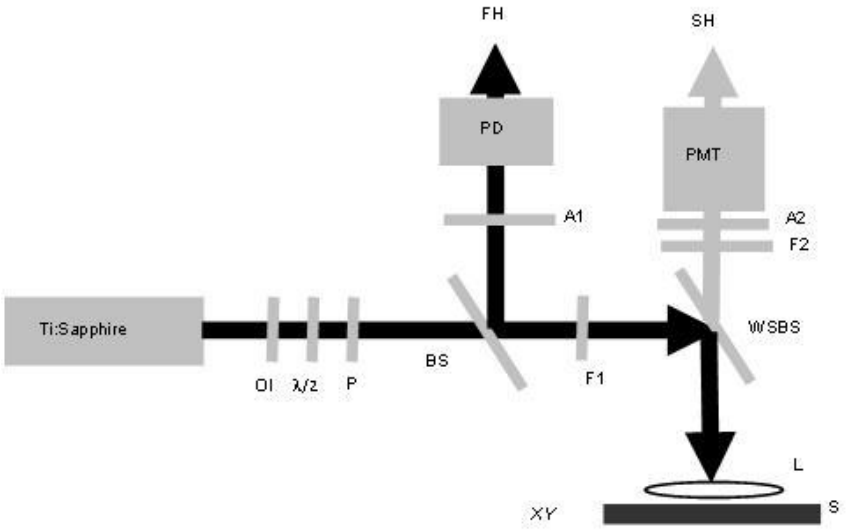

Figure 4. Schematic of the experimental setup. OI: optical isolator, λ/2: halfwave-plate, P: polarizer, BS: beam splitter, F1 and F2: filters, WSBS: wavelength selective beam splitter, L: objective, S: sample, XY: stage, A1 and A2: analysers, PMT photomultiplier tube, and PD: photodiode

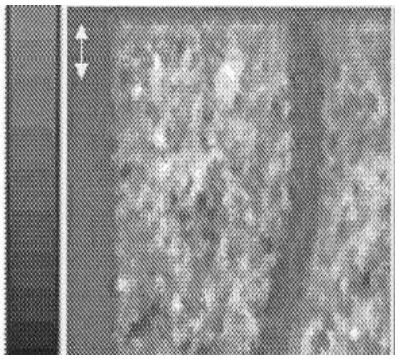

Figure 5. Sample structure. It consists of a high density scattering regions composed of gold bumps (~ 70 nm high) randomly distributed over a thin (~50 nm) gold film

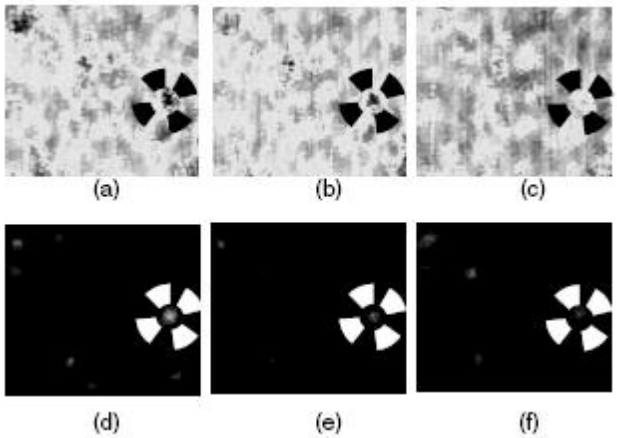

Figure 6. Gray scale FH (a-c) and corresponding SH (d-f) images of 8x8μm^2 obtained for 770 (a,d), 780 (b,e),and 790 (c,f) nm of the FH wavelength. The polarization of the FH (incident) and the SH (detected) signal were both kept vertical with respect to the presented images respectively. The maximum of the SH signal was 1200 cps (d). Representative dark (a-c) and bright (d-f) spots were enclosed in circles for better visualization

It consisted of a scanning optical microscope in reflection geometry built on the base of a commercial microscope and a computer controlled two-dimensional (*XY*) translation stage. The *XY* stage is able of moving in steps down to 50 nm with the accuracy of 4 nm within a scanning area of 25x25 mm^2. A mode-locked pulsed Ti-Sapphire laser tunable was used in the range of 730-920 nm with pulse duration of ~200 fs, 80 MHz of repetition rate and an average output power of ~300 mW. The linearly polarized light beam from the laser is used as a source of sample illumination at the fundamental harmonic (FH) frequency. The laser beam pass through a wavelength selective splitter and it is focused at normal incidence on the sample surface (spot size ~1μm) with a Mitutoyo infinity-corrected long working distance x 100 objective. In order to avoid thermal damage on the sample, the average incident power was kept at the level of ~20 mW (intensity at the surface ~2 ×10^6 W/cm^2). The sample reflects the FH and the generated SH radiation back to the same objective. The FH and SH signals are separated with the beam splitter and, after passing the appropriated filters and polarizers, detected with a photodiode and a photomultiplier tube respectively. Finally both

signals are recorded as a function of the scanning coordinate obtaining, simultaneously, FH and SH images of the sample surface. The resolution of the SHSOM was evaluated in ~0.7μm using domain walls of an electric field poled $KTiOPO_4$ quasi-phase matching crystal [23]. The sample under investigation was fabricated by using thermal evaporation and electron beam lithography techniques (more information about the procedure is found in Ref. [24]). The final sample structure consists of high density scattering regions composed of gold bumps (~ 70 nm high) randomly distributed over a thin (~50 nm) gold film (Figure 5). The scattering regions density is approximately 50 scatterers per $1\mu m^2$ and contains 2μm-wide channels free from scattereres that were used for investigations of guiding of SPPs [24]. There were recorded simultaneously FH and SH images of a dense scattering region in the wavelength range of 750-830 nm. The overall behavior of images of the same particular signal was very similar (Figure 6 a-f). In general one can appreciate bright and dark regions which are a collection of small and round bright spots similar to those reported as evidence of localized SPPs [4]. The presence of the observed spots suggested that the total detected FH radiation can be considered as a superposition of the FH beam reflected from the flat gold surface and the FH field scattered by strongly interacting gold bumps. The latter contribution is related to the regime of multiple scattering of the light which exhibits strong polarization and frequency dependence [4] and can be expected to occur, for example, due to localization of resonant dipolar excitations at nanostructured surfaces. In general, one should expect the most efficient excitation for well-localized modes with one strong field maximum. Light scattering via excitation of such a mode (arising from the nano particles) should be similar to the dipole scattering resulting in the excitation of SPP modes. SPPs are scattered, in turn, in the surface plane and into the substrate as well as absorbed due to the internal damping. These processes contribute to the decrease of the total flux in the direction of reflection and, thereby, formation of dark spots (see spots enclosed in circles in Figure 6 a-f). The images showed a noticeable re-distribution of the intensity. The bright spot (enclosed in circle) seen clearly in Figure 6d was re-distributed in Figure 6f. Taking this into account, one can claim that the bright spots were not correlated with surface defects since they show illumination wavelength dependence. It is also possible to notice that dark FH spots coincide with bright SH ones (enclosed spots in Figure 6 a-f). About this fact, an explanation can be formulated. Excitation of an FH eigenmode (leading to the local FH enhancement) results in a strong SH signal only if the SH field, which is associated with the generated nonlinear polarization, is further enhanced due to excitation of the corresponding SH eigenmode. That is to say, FH and SH eigenmodes should overlap in the surface plane. However, in general, such a correspondence is very difficult to observe because of the relative low contrast of FH images.

5. SPP SCALAR MULTIPLE SCATTERING MODEL

Typically, elastic scattering of SPP and related plasmonic phenomena (e.g weak and strong localization) have been investigated by direct evaluation of the near-field optical image obtained at the place where the SPP is being resonantly excited [3]. This task could be numerically well complemented by using a SPP scalar multiple scattering model. Such model is based on two assumptions:

(i) The elastic SPP scattering is dominant with respect to the inelastic scattering
(ii) The SPP scattered by each scatterer represents an isotropic cylindrical SPP.

These assumptions allow one to avoid some of the complicated mathematical treatments involved in the problem of SPP scattering by surface inhomogeneities [25]. The field at a point in the plane pointed at by the vector $\boldsymbol{r}$ is given by:

$$E(\boldsymbol{r}) = E_0(\boldsymbol{r}) + \sum_{j=1}^{N} \alpha_j E(\boldsymbol{r}_j) G(\boldsymbol{r},\boldsymbol{r}_j), \tag{7}$$

where is $E_0(\boldsymbol{r})$ the incident field, α_j is the effective polarizability of the jth dipole, $E(\boldsymbol{r}_j)$ is the self–consistent field at the site of the jth dipole $G(\boldsymbol{r},\boldsymbol{r}_j)$ is the field propagator, describing the scattered propagation of the scattered field from the jth dipole located at the source point $\boldsymbol{r}_j$ to the observation point $\boldsymbol{r}$. The self-consistent field to each dipole $E(\boldsymbol{r}_j)$ can be determined as

$$E(\boldsymbol{r}_j) = E_0(\boldsymbol{r}_j) + \sum_{l=1, l\neq j}^{N} \alpha_l E_l(\boldsymbol{r}_j) G(\boldsymbol{r}_j,\boldsymbol{r}_l). \tag{8}$$

The total field at the site of the dipole j is the incoming field at the site of the scatterer and the sum of the scattered fields from all dipoles surrounding dipole j. The field in (8) then has to be inserted in (7) to find the total field at a point in the plane. The field propagator is given as:

$$G(\boldsymbol{r},\boldsymbol{r}_j) = \frac{1}{4} H_0^{(1)}\left(\beta\left|\boldsymbol{r}-\boldsymbol{r}_j\right|\right), \tag{9}$$

where $H_0^{(1)}$ is the zero-order Hankel function of first kind and β is the propagation constant for the SPPs. The Hankel function first kind of order n is defined as

$$\begin{aligned} H_0^{(1)}\left(\beta\left|\boldsymbol{r}-\boldsymbol{r}_j\right|\right) &= J_n\left(\beta\left|\boldsymbol{r}-\boldsymbol{r}_j\right|\right) + iY_n\left(\beta\left|\boldsymbol{r}-\boldsymbol{r}_j\right|\right) \\ &= J_n\left(\beta\left|\boldsymbol{r}-\boldsymbol{r}_j\right|\right) + \\ &\quad i\frac{J_n\left(\beta\left|\boldsymbol{r}-\boldsymbol{r}_j\right|\cos(n\pi)\right) - J_{-n}\left(\beta\left|\boldsymbol{r}-\boldsymbol{r}_j\right|\right)}{\sin(n\pi)}. \end{aligned} \tag{10}$$

where $J_n\left(\beta\left|\boldsymbol{r}-\boldsymbol{r}_j\right|\right)$ is the Bessel function of the first kind and, $Y_n\left(\beta\left|\boldsymbol{r}-\boldsymbol{r}_j\right|\right)$ is the Bessel function of the second kind, and n is the order. Often it is appropriate and easier to use the farfield approximation for the Hankel Function. The farfield corresponds to large values of the argument, and the farfield approximation reads for large arguments:

$$H_0^{(1)}\left(\beta\left|\mathbf{r}-\mathbf{r}_j\right|\right)\approx\sqrt{\frac{2}{\pi}}e^{-i\frac{\pi}{4}}\frac{e^{i\beta\left|\mathbf{r}-\mathbf{r}_j\right|}}{\sqrt{\beta\left|\mathbf{r}-\mathbf{r}_j\right|}}. \tag{11}$$

The estimation of the magnitude of α, the effective polarizability of the individual scatterers has been done by fitting α such that the calculated (parabolic) interference pattern generated by an individual scatterer has the same contrast of an experimental (near-field) intensity distribution generated in analogue form [4]. Thus, $\alpha = 3$ was a typical value that was used in the calculations. The SPP elastically scattered has been simulated by using a light wavelength $\lambda = 633nm$ and a dielectric constant $\varepsilon = -16+i$ which corresponds to a silver film at the wavelength of illumination. The calculated total elastic cross section of the scatterer (with $a = 3$) was found to be: $\sigma = 0.22\ \mu m$. The value of σ can be used as a check of the estimation of α, i.e., for a symmetric surface defect considered theoretically [25] the same cross section would correspond (in the first Born approximation) to a scatterer of 0.1 μm of height and 0.7mm of radius. As a first case, we have considered the scattering from a single particle. The propagation constant for the SPPs is taken real, so no damping across the surface is presented. Since only a single particle is included, there is no scattering contribution from neighbors, and (7) therefore reduces to the following:

$$E\left(\mathbf{r}_j\right)=E_0\left(\mathbf{r}_j\right). \tag{12}$$

Now a plane wave of unit amplitude travelling from left to right is incident on the nano-particle that is:

$$E_0\left(\mathbf{r}_j\right)=e^{i\beta x_j}. \tag{13}$$

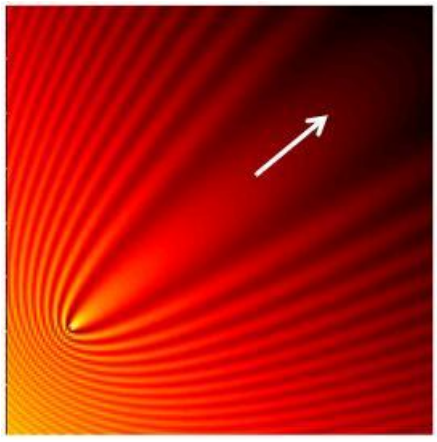

Figure 7. Intensity distribution of a single particle calculated with the scalar model. The illumination wavelength, $\lambda_0 = 750nm$ and the radius of the scatterer is $r = 50nm$. The white arrow indicates the SPP incident direction

With the use of (12) and (13), the far-field approximation for the Hankel function in (10) and (11), the total field from a plane wave and spherical wave can be written:

$$E(\mathbf{r}) = e^{i\beta x} + \alpha e^{i\beta x_j} \cdot \frac{i}{4}\sqrt{\frac{2}{\pi}} e^{-i\frac{\pi}{4}} \frac{e^{i\beta|\mathbf{r}-\mathbf{r}_j|}}{\sqrt{\beta|\mathbf{r}-\mathbf{r}_j|}}. \tag{14}$$

Leading right to the intensity:

$$I(\mathbf{r}) = |E(\mathbf{r})|^2 = 1 + \frac{\alpha^2}{8\pi}\left(\beta|\mathbf{r}-\mathbf{r}_j|\right)^{-1} + \frac{\alpha}{2}\sqrt{\frac{2}{\pi}}\sin\left(\begin{matrix}\beta(x-x_j)+\ldots \\ +\frac{\pi}{4}-\beta|\mathbf{r}-\mathbf{r}_j|\end{matrix}\right). \tag{15}$$

For maximum intensity the sine oscillation has to equal 1, then:

$$\beta\left(x - x_j - \sqrt{(x-x_j)^2 + (y-y_j)^2}\right) + \frac{\pi}{4} = \frac{\pi}{2} + n2\pi. \tag{16}$$

where n is an integer. For the sake of simplicity, the position of the particle $r_j(x_j,y_j)$ is placed at the origo. Bearing this in mind and using b the SPP propagation constant now reads for $n > 0$:

$$x\left(1+\frac{1}{8n}\right) = \frac{y^2}{2n\Lambda_{SPP}} - \frac{n\Lambda_{SPP}}{2} - \frac{\Lambda_{SPP}}{8} - \frac{\Lambda_{SPP}}{128n}. \tag{17}$$

For growing values of n the last term on the left hand side and the last two terms on the right hand side becomes vanishing compared the rest. Then, one can see, that a parabolic fringes in y with a distance of $\Lambda_{SPP}/2$ between terms is expected. Figure 2 shows a simulation of (x) for a single nano-particle in a silver/air interface, where one can see that the fringes indeed have parabolic shape.

6. SPP VECTORIAL MULTIPLE SCATTERING MODEL

Despite the apparent success, the scalar model presents limitations, one of them being that the effective polarizability of an individual scatterer is a phenomenological quantity which is difficult to relate to scatterers parameters such as size and dielectric susceptibility. The model was extended into a vector dipolar multiple-scattering theory and used, among other things, to calculate SPP scattering produced by band-gap structures [8]. The approach entails point-like dipolar scatterers interacting via SPPs so that the multiple-scattering problem in question can be explicitly formulated, making it very attractive for modelling of

SPP plasmonic phenomena. The validity of the model was established for relatively large inter-particle distances, whereas for smaller distances it was more accurate to use a total Green's tensor and include multipolar contributions in the scattered field. The self-consistent polarization of each scatterer established in the process of multiple scattering is obtained by solving the following equation:

$$\boldsymbol{P}_i = \alpha_i \cdot E^0(\boldsymbol{r}_i) + \frac{k_0^2}{\varepsilon_0} \sum_{n \neq i} \alpha_i \cdot G(\boldsymbol{r}_i, \boldsymbol{r}_n) \cdot \boldsymbol{P}_n \quad . \tag{18}$$

where $\boldsymbol{P}_i$ is the polarization of the particle *i*, α is the polarizability tensor for particle *i* with the multiple scattering between the particle and the metal surface taken into account E^0 is an incoming electric field, k_0 is the free space wave number, λ_0 is the vacuum permittivity and $G(\boldsymbol{r}_i,\boldsymbol{r}_n)$ is the Green´s tensor for the reference structure (total field propagator). The Green`s tensor $G$ is the sum of a direct contribution $G_d$, in this case the free space Green`s tensor, and an indirect contribution G_s that describes both reflection from the metal/dielectric interface and excitation of SPPs. The incoming E^0 describes a Gaussian SPP field impinging on the arrangement of scatterers. For a spherical particle made of the same metal as the substrate, the polarizability tensor is given by

$$\boldsymbol{\alpha} \approx \left[\boldsymbol{I} - \frac{\varepsilon - 1}{\varepsilon + 1} \frac{\varepsilon - 1}{\varepsilon + 2} \left(\frac{1}{8} \hat{x}\hat{x} + \frac{1}{8} \hat{y}\hat{y} + \frac{1}{4} \hat{z}\hat{z} \right) \right]^{-1} \cdot \boldsymbol{\alpha}^0 . \tag{19}$$

where $\boldsymbol{I}$ is the unit dyadic tensor, ε is the metal dielectric constant, $\hat{x}, \hat{y}, \hat{z}$ are unit vectors in a Cartesian coordinate system with $\hat{z}$ being perpendicular to the air–metal interface, and $\boldsymbol{\alpha}^0 = \varepsilon_0 \boldsymbol{I} 4\pi a^3 (\varepsilon - 1)/(\varepsilon + 2)$ is the free space polarizability tensor in the longwave electrostatic approximation with a being the sphere radius. The polarizations and the total field,

$$\boldsymbol{E}(\boldsymbol{r}) = \boldsymbol{E}^0(\boldsymbol{r}) + \frac{k_0^2}{\varepsilon_0} \sum_n \boldsymbol{G}(\boldsymbol{r}, \boldsymbol{r}_n) \cdot \boldsymbol{P}_n \quad . \tag{20}$$

can be calculated using the appropriate Green`s tensor for the reference structure $G(\boldsymbol{r},\boldsymbol{r}_n)$. Considering both the source and observation points being close to a meal surface but far away from each other, one can approximate the total Green dyadic (which includes the direct and indirect terms) with the part of the indirect Green dyadic concerned with the excitation of SPPs [8]. In this approximation which is actually asymptotically correct as the in-plane separation of source and observation points increases towards infinity, the Green dyadic can be represented by

$$G_{SPP}(r,r_n) \approx \alpha_{zz}(\lambda) e^{iK_z(z+h)} H_0^1(K_\rho \rho) * [\hat{z}\hat{z} + \cdots$$
$$(\hat{z}\hat{\rho} - \hat{\rho}\hat{z}) \frac{K_z}{K_\rho} - \hat{\rho}\hat{\rho} \left(\frac{K_z}{K_\rho} \right)^2], \tag{21}$$

where H_0^1 is the zero-order Hankel function of the first kind, $\rho = |r_{II} - r'_{II}|$, $\hat{\rho} = (r_{II} - r'_{II})/\rho$, with II referring to the projection of the radius vector on the xy plane, which coincides with the metal air interface, and z refers to the height of observation point r above de surface, while h refers to the height of the source point r' Finally, K_z and K_ρ are the components of the three-dimensional SPP wave vector.

$$K_\rho = k_0 \sqrt{\frac{\varepsilon}{\varepsilon + 1}}. \tag{22}$$

$$K_z = \sqrt{k_0^2 - K_\rho^2}. \tag{23}$$

and

$$\alpha_{zz}(\lambda) = \frac{K_\rho}{2} \left(\sqrt{\varepsilon} \left(1 - \frac{1}{\varepsilon^2} \right) \frac{1+\varepsilon}{\varepsilon} \right)^{-1}. \tag{24}$$

The complete analysis of the validity domain of such an approximation is beyond the scope of this work and can be found elsewhere [8]. As previously mentioned, a single circular nanoparticle is assumed to scatter light as cylindrical waves, so no preferred direction of scattering is presented. By placing particles in line of nano-arrays, a common plane wavefront of the scattered light can be achieved. From an application point of view, it seems obvious to exploit line arrays to reflect the wavefront to the applied field in order to make a mirror effect. The idea has been modelled for a line array of $3\mu m$ length and whose inclination compared to the applied field is 45^0 [26]. The line arrays are far from being perfect mirrors since much of the incident light may pass through the structures. This fact can be compensated for by placing an array of lines that satisfy the Bragg condition, $2d\sin\theta = n\lambda$, where d is the separation distance, θ is the angle the beam makes with the mirror and n is a whole number. Here, we chose an inter-particle distance of 200nm and an inter-line separation of 350nm with an incident beam angle of 60^0. The simulation has been performed with an incoming Gaussian beam of the form:

$$E_0 = e^{\left(-\frac{y^2}{w^2} + i\beta x \right)}. \tag{25}$$

The incoming wavelength, λ_0, the beam waist, w, and the particle radii, r were fixed to $750nm$, $2\mu m$, and $60nm$ respectively. Figure 6 shows the mirroring effect from the nano-particles. However, much of the signal is still transmitted. This fact is expected when only a few particles lines are used. With many layers of particles in an array, it is possible to obtain almost all of the reflected power when certain wavelengths of the incoming beam. That is the principle of the SPP band gap (SPPBG) structures. SPPBG phenomena are beyond the scope of this work but an overview can be found in Ref [8].

7. NANO OPTICS OF SURFACE PLASMON POLARITONS

Two-dimensional optics of surface plasmon polaritons is an exciting novel area. In this context, there exists a revolution in scientific and technological aspects in specific phenomena such as enhancement of an optical signal at a desirable surface place [1,2], waveguiding of SPP [1,2], and in a more general form in integrated optics. Experimental observations on nano-bumps acting as a nano-lens (focusing the SPP field) yielded conclusions about optimal parameters for a good efficiency of SPP nano components. The observations suggested that nano scatterers sufficiently large in size and with smooth borders maximize their strength and preserve an adiabatic perturbation. Thus, some of the first plane (Figure 9) and corner square [26] nano mirrors were successfully reported.

Another plasmonic device, realizable by a certain array structure of nano-particles, is a focusing micromirror. We show numerically such a possibility. The concept is to place the particles along a parabolic curve $(y-y_0)^2 = 4F(x-x_0)$ where the coordinate (x_0, y_0) is located at the bottom of the mirror, F is the focal length and x is along the optical axis. In principle, this works for the two-dimensional case of SPP propagation in the same way as the three-dimensional case of a parabolic screen of a solar cooker, which concentrates reflected solar light at a cooking pot. Hence, at the point $(x_0 + F, y_0)$ a concentration of light is expected. In Figure 10, we simulated a nanomirror with $F = 8\mu m$ and where the focusing effect was clearly seen. For applications matters, focusing nano-mirrors give the possibility to enhance SPP signal locally in a controllable way. One can think to exploit that feature in, for example, biosensors, and surface enhanced Raman spectroscopy.

7. TWO-DIMENSIONAL OPTICS WITH SURFACE ELECTROMAGNETIC MICROWAVES

In the microwave range the mechanical designs as well as the precision requirements are not as demanding as in the optical range. Taking advantage of that fact, experimental approaches for a wavelength, λ, of 2.85 cm. were proposed as a check of potential (two-dimensional) nano-components [13]. Several spheres were aligned keeping approximately $\lambda/2$ distance of separation between them. Thus, distinct two-dimensional microwave components were fabricated e.g.: a 5-scatterer two-dimensional line mirror (Figure 8a,b), and a curved mirror focusing that reflected signal at 2.5 cm distance from the mirror (Figure 9a,b).

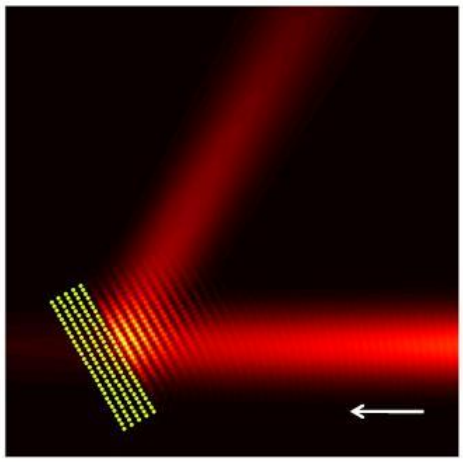

Figure 8. Intensity distribution of a multiline mirror with 5 lines of 30 nano-particles with radius r = 63*nm* Inter-particle and inter-layer distances are 200 and 350*nm* respectively. The incoming SPP beam has a wavelength, λ_0 = 750*nm* . The white arrow indicates the SPP incident direction

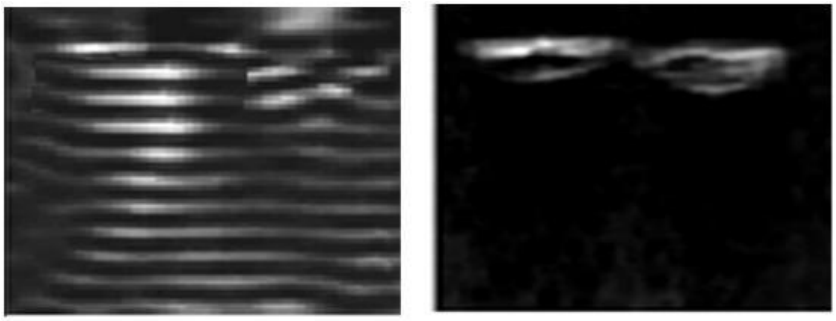

(a) (b)

Figure 9. Gray-scale topographical a) and near-field optical images b) 4.4×4.3 μm^2 of a potential plane nano-mirror. In the figure, the SPP travels from bottom to top

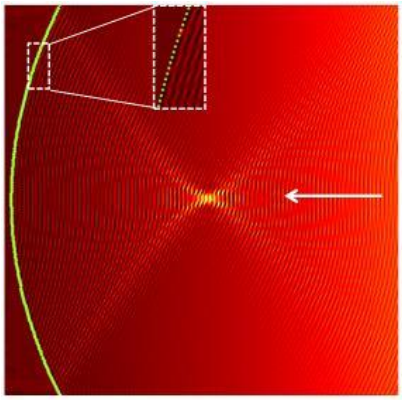

Figure 10. Intensity distribution map in an area of 30x30μm^2 calculated for a curved micromirror with a focal length F = 15μm and composed of 140 nano-particles with inter-particle distance of 220*nm*. The dotted line represents the curved nanomirror. All else is as in Figure 8

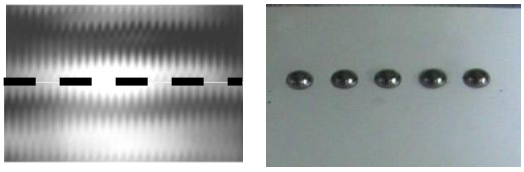

(a) (b)

Figure 11. Gray-scale near-field image of 4.5 x 10 cm^2 a) due to the elastic scattering of an evanescent microwave mode travelling from bottom to top a) on the line of scatterers placed along a wax surface prism and corresponding surface digital picture b). The dot line in a) helps to distinguish the boundary of evanescent wave and line of spheres interaction

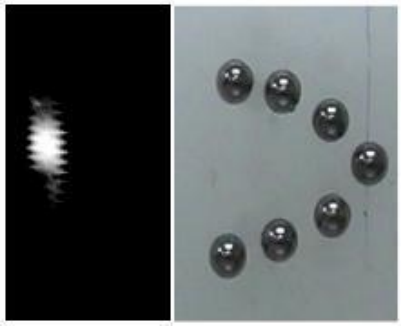

Figure 12. Gray-scale near-field image of 4 x 6 cm^2 due to the elastic scattering of an evanescent microwave mode travelling from left to right on the parabolic line of scatterers placed along a wax surface prism a), and corresponding surface digital picture (not in scale) b)

The image for the line mirror showed the interference between a specular reflected evanescent microwave and the incident one. The behaviour, for the line mirrors, was not as good as it had to be. For example in Figure 11a,b the line mirror does not completely backward reflect the incident evanescent field (travelling from bottom to top in the horizontal position) as one would expect from a normal incidence. Concerning the focusing mirror (Figure 12a,b), ideally a focusing mirror should consist of scatterers placed along a parabolic curve $y^2 = 4Fx$ where (x, y) is the orthogonal system of coordinates in the surface plane, the x axis is oriented along the optical axis and F is the focal length. Based on that, a mirror with F = 2.5 cm was fabricated. The operational principle of the component resulted rather satisfactory. For example the expected focusing was exhibited along the axis of the mirror.

8. CONCLUSION

In this chapter, the basic ideas of SPPs and experimental results concerning the phenomenon of SPP localization were reviewed. As far as the SPP localization phenomenon is concerned, it should be stressed that there are many basic and technological aspects that have to be yet explored. The physics behind such a phenomenon is not simple. For instances,

the influence of dissipation and wave-wave interaction are not clarified yet [27]. In another hand, results concerning the modelling of plasmonic phenomena were presented. Even though in the last years, there has been a great progress in the understanding of plasmonic phenomena, there exists not at the moment a complete theoretical model to deal with such studies. In that context, a relative simple scalar multiple SPP scattering model was presented. Nano-particles were considered in a two- dimensional geometry as isotropic point-like particles characterized by their effective polarizabilities. The scalar model has limitations on the accuracy of numerical results. For example, the effective polarizability of an individual particler is a phenomenological quantity that is difficult to relate to particle parameters such as size, susceptibility, etc. The scalar approach was extended into a vectorial dipolar model for SPP multiple scattering and used to model the operation of a SPP multiline mirror whose main element represented individual scatterers lined up and equally spaced. One can try to further improve this model by, for example, developing another (but analytical as well) approximation of the Green´s tensor for relatively small inter-particle distances. In the area of surface plasmon polariton nano-optics many features have already been clarified. The progress in both theoretical and experimental aspects has significantly increased with the advent of the near-field optical microscopy. Thus, nano-particles were used to create almost any kind of conceivable SPP nanocomponent such as a parabolic nano-mirrors. During the course of the research, several devices composed of a set of nano-scatterers have been numerically simulated and its stability (to geometric parameters) and dispersion dependence were studied in detail. The corresponding experimental results demonstrated that the model is accurate enough and that can be used, in straightforward manner, to design SPP nano-components. Finally, we have designed and constructed a stand-alone SNMM, including electronics and software, and demonstrated that it works. The SNMM showed capabilities for imaging of evanescent microwaves. The technique can be used, with certain limitations, as a check for testing potential micro and nano components assembled of individual scatterers, e.g., beam-splitters and interferometers. We conduct further investigations in this area.

ACKNOWLEDGEMENT

Two of us (R.C. and V.C.) acknowledge financial support from CONACyT Mexico, project No 123553.

REFERENCES

[1] Surface Plasmon Nanophotonics; Eds, Brongersma Mark L.; Kik, Pieter G.; *Series in Optical Science*s; Springer-Verlag: Berlin, GR, 2007, Vol. 131, 271.

[2] Plasmonic Nanoguides and Circuits, Ed, Sergey I. Bozhevolnyi. Pan Stanford Publishing, *World Scientific*, Singapure, 2008, Vol 1, 452.

[3] Near-Field Optics and Surface Plasmon Polaritons, Eds. Kawata, Satoshi; Ohtsu, Motoichi; Irie, Masahiro; Series: *Topics in Applied Physics*, Springer-Verlag: Berlin, GR, 2001, Vol 10, 210.

[4] V.Coello, *Surf Rev and Lett*, 2008, Vol 15, 867-879.

[5] Maier, Stefan Alexander. Plasmonics: Fundamentals and Applications; *Springer-Verlag: Berlin, GR*, 2007, XXV, 223.
[6] Bozhevolnyi, SI; Coello, V; *Phys. Rev, B*. 1998, Vol 58, 10899-10910.
[7] Bozhevolnyi, SI; Volkov, VS. Opt. *Commun*, 2001, Vol 198, 241-245.
[8] Søndergaard, T; Bozhevolnyi, SI; Phys Rev, B. 2003, Vol 67, 165405-165412.
[9] Coello, V; Søndergaard, T; Bozhevolnyi, SI. Opt. *Comm*, 2004, Vol 240, 345-350.
[10] Ash, E; Nicholls, G. *Nature*, 1972, Vol 237, 510- 512.
[11] Wei, T; Xiang, XD; Wallace-Freedman, WG; Schultz, PG. *Appl. Phys. Lett*, 1996, Vol 68, 3506-3508.
[12] Vlahacos, CP; Black, RC; Anlage, SM; Amar, A; Wellstood, FC. *Appl. Phys. Lett*, 1996, Vol 69, 3272-3274.
[13] Coello, V; Cortes, R; Villagomez, R; Lopez, R; Martinez, C. *Rev. Mex. de Fís*, 2005, Vol 51, 426-430.
[14] Raether, H. Surface Plasmons, *Springer Tracts in Modern Physics*, 1998, Springer, Berlin, GR, Vol. 111, 136.
[15] de Fornel, F. *Evanescent Waves: From Newtonian Optics to Atomic Optics*; Springer-Verlag: Berlin, GR, 2001, I, 282.
[16] Drezet, A; Hohenau, A; Stepanov, AL; Ditlbacher, H; Steinberger, B; Aussenegg, F; Leitner, A; Krenn, J. *Plasmonics*, 2006, Vol 1, 141-145.
[17] Kim, DS; Hohng, SC; Malyarchuk, V; Yoon, YC; Ahn, YH; Yee, KJ; Park, JW; Kim, J; Park, QH; Lienau, C. *Phys. Rev. Lett*, 2003, Vol 91, 143901-143904.
[18] Devaux, E; Ebbesen, TW; Weeber, JC; Dereux, A. *Appl. Phys. Lett*, 2003, Vol 83, 4936-4939.
[19] Radko, IP; Bozhevolnyi, SI; Evlyukhin, AB; Boltasseva, A. *Optics Express*, 2008, Vol 15, 6576-6582.
[20] Radko, IP; Evlyukhin, AB; Boltasseva, A; Bozhevolnyi, SI. *Optics Express*, 2008, Vol. 16, 3924-3930.
[21] Coello, V; Beermann, J; Bozhevolnyi, S. physica status solidi (c), 2003, vol.0, 3070-3074.
[22] Bozhevolnyi, SI; Beermann, J; Coello, V. *Phys. Rev. Lett*, 2003, Vol 90, 197403-197406.
[23] Vohnsen, B; Bozhevolnyi, SI. *J. Microscopy*, 2001, Vol 202, 244-249.
[24] Bozhevolnyi, SI; Volkov, VS; Leosson, K. *Phys. Rev. Lett*, 2002, Vol 89, 186801-186804.
[25] Shchegrov, AV; Novikov, IV; Maradudin, AA. Phys. *Rev. Lett*, 1997, Vol 78, 4269-4272.
[26] Bozhevolnyi, SI; Coello, V. *Phys. Rev. B*, 1998, Vol. 58, 10899-10910.
[27] John, S; in Sheng Scattering, P. and Localization of Clasical Waves in Random Media, *World Scientific, Singapore*, 1990, 1.